ANNALS OF GEOPHYSICS, 66, 5, PA528, 2023; doi:10.4401/ag-9026
OPEN ACCESS

Ionospheric equivalent slab thickness ingestion into the NeQuick model

Alessio Pignalberi[*,1], Bruno Nava[2], Marco Pietrella[1], Michael Pezzopane[1], Pierdavide Coïsson[3], Claudio Cesaroni[1]

(1) Istituto Nazionale di Geofisica e Vulcanologia, Via di Vigna Murata 605, 00143, Rome, Italy
(2) The Abdus Salam International Centre for Theoretical Physics, Strada Costiera , 34151, Trieste, Italy
(3) Université Paris Cité, Institut de Physique du Globe de Paris, CNRS, 75005, Paris, France

Article history: received October 17, 2023; accepted December 20, 2023

Abstract

The ionospheric equivalent slab thickness (τ), defined as the ratio of the vertical total electron content (vTEC) to the ionospheric F2-layer electron density maximum (*Nm*F2), is a parameter providing useful information on the shape of the vertical electron density profile. However, the use of this information is of difficult practical application in empirical ionosphere models, such as the NeQuick, because by design they do not explicitly include τ as a modelling parameter. In this work, we investigated the opportunity of using measured τ values to improve the empirical modelling of the ionosphere vertical electron density profile by NeQuick. Measured τ values were obtained through *Nm*F2 observations and vTEC measurements obtained between 2001 and 2019 by an ionosonde and a ground-based GNSS receiver, respectively, co-located at Rome ionospheric station (41.8° N, 12.5° E; Italy). NeQuick τ was obtained as the ratio between modelled *Nm*F2 and vTEC values, the latter calculated by integration of the vertical profile. As a first step, τ values modelled by NeQuick were compared with corresponding values measured at Rome station to highlight diurnal, seasonal, and solar activity differences. Then, measured τ values were ingested in NeQuick through a three-parameter assimilation procedure which first assimilates F2-layer peak characteristics to constrain the F2-layer anchor point, and then assimilates vTEC to optimize the F2-layer shape through the NeQuick F2-layer thickness parameter, namely $B_{2\mathrm{bot}}$. The assimilation procedure provides information on how the NeQuick $B_{2\mathrm{bot}}$ has to be modified to match measured τ values, and then on how the shape of the F2-layer profile has to be changed accordingly. Our results highlight that, in many cases, the NeQuick $B_{2\mathrm{bot}}$ has to be increased to match observations, which has implications on the modelling of the NeQuick bottomside and topside effective scale heights.

Keywords: Ionospheric equivalent slab thickness; NeQuick model; Ionosphere modelling; Data assimilation; Effective scale height

1. Introduction

The ratio of the vertical total electron content (vTEC) to the ionospheric F2-layer electron density maximum (*Nm*F2) defines the ionospheric equivalent slab thickness (τ). This parameter describes the equivalent thickness of an ideal ionospheric slab with a uniform electron density equal to *Nm*F2 and whose total electron content is equal to vTEC [Titheridge, 1973]. Ionospheric vertical electron density profiles with a small τ ($\leq$ 300 km) are relatively thin around the F2-layer peak, while profiles with a high τ ($\geq$ 300 km) are relatively thick around the F2-layer peak. As a consequence, τ characterizes the shape of the vertical electron density profile around the F2 region, thus providing information about the plasma distribution between the bottomside and the topside ionosphere [Pignalberi et al., 2022a].

Since its definition in the 1960s [Bauer, 1960; Garriott, 1960; Ross, 1960; Roger, 1964; Garriott et al., 1965], the behavior of τ has been deeply investigated by many authors in terms of its spatial, diurnal, seasonal, solar and geomagnetic activity variations [Titheridge, 1973; Davies and Liu, 1991; Fox et al., 1991; Jayachandran et al., 2004; Leitinger et al., 2004; Gulyaeva and Stanislawska, 2005; Jin et al., 2007; Stankov and Warnant, 2009; Guo et al., 2011; Huang et al., 2016; Jakowski et al., 2017; Pignalberi et al., 2021, 2022a]. Moreover, relations between τ and several neutral and plasma parameters were highlighted in the past. For instance, its link with the neutral vertical scale height and temperature [Wright, 1960; Hibberd and Ross, 1966; Titheridge, 1973; Jakowski et al., 2017], and with the plasma temperature [Amayenc et al., 1971; Furman and Prasad, 1973; Stankov and Jakowski, 2006]. Since τ relates vTEC with *Nm*F2, it has also found practical application in models based on the data-assimilation of vTEC from ground-based global navigation satellite system (GNSS) receiver networks. In fact, it allows predicting *Nm*F2 at locations where only vTEC observations from ground-based GNSS receivers are available [Krankowski et al., 2007; Gerzen et al., 2013; Pignalberi et al., 2019]. Recently, a global description of τ has been made possible through empirical [Jakowski and Hoque, 2021] and data-assimilation models [Fron et al., 2020; Galkin et al., 2022]. For a thorough and complete review of the main features, studies, and models about the ionospheric equivalent slab thickness, please refer to the review paper by Pignalberi et al. [2022a].

In this work, we focus on the use of the ionospheric equivalent slab thickness for an empirical modelling of the ionosphere. Specifically, we aim at ingesting measured τ values into the NeQuick empirical ionospheric model [Nava et al., 2008] to improve the description of the vertical electron density profile shape. This work is motivated by the fact that, currently, the most representative empirical ionospheric models, i.e., the International Reference Ionosphere [IRI, Bilitza et al., 2022] and NeQuick [Nava et al., 2008], do not use τ as a modelling parameter and do not even directly provide τ as output. However, since these models provide the vertical electron density profile up to GNSS satellites altitudes, it is possible to obtain modelled τ values as a by-product of modelled *Nm*F2 and vTEC values. Then, a comparison between measured and modelled τ values is possible. In this study, such comparison has been performed by using data recorded at the mid-latitude station of Rome (41.8° N, 12.5° E; Italy) and the NeQuick model. In view of a potential application of τ in empirical ionosphere modelling, it is interesting to investigate if and how the information about τ can help the modelling of the shape of the vertical electron density profile. For this reason, we will show how the F2-layer thickness parameter used by NeQuick ($B_{2\mathrm{bot}}$) has to be modified to agree with measured τ values. To do so, we will apply the NeQuick three-parameter data-ingestion procedure developed by Nava et al. [2011], based on the ingestion of measured *Nm*F2, *hm*F2, and vTEC values in NeQuick. This analysis will give us clues on how to improve the NeQuick description of the F2 region shape, i.e., the $B_{2\mathrm{bot}}$ bottomside thickness parameter, through measured τ values. Since in NeQuick the bottomside and the topside thickness parameters are linked, a change in $B_{2\mathrm{bot}}$ will also affect the description of the topside profile shape, and in turn the modelled vTEC. As a consequence, this analysis will also point out what are the current weaknesses in the NeQuick modelling of the topside ionosphere and how to improve it by working on the NeQuick topside thickness parameter, i.e., the topside effective scale height [Pignalberi et al., 2020a, 2022b].

Section 2 first describes the vTEC and *Nm*F2 datasets used to derive τ for the mid-latitude station of Rome, and how data are analyzed to obtain the main climatological features of vTEC, *Nm*F2, and τ. The same section describes how NeQuick models τ, and how measured parameters are ingested in NeQuick to match the observed τ values. Section 3 collects the results of the comparison between vTEC, *Nm*F2, and τ values measured at Rome station and those modelled by NeQuick. After this comparison, the results about the ingestion of measured values in NeQuick to calculate the correction factor to be applied to the NeQuick $B_{2\mathrm{bot}}$ are presented. Section 4 discusses the results and implications for the empirical modelling of the vertical electron density profile made by NeQuick. Finally, Section 5 draws the conclusions and possible future developments.

2. Data and method

2.1 Slab thickness from co-located ionosonde and GNSS receiver observations

Measured τ values are obtained by applying the procedure described in papers by Pignalberi et al. [2021, 2022a], to which the reader can refer for the full details and additional information.

To calculate τ we use a ground-based GNSS receiver co-located with an ionosonde, both located in the Rome (41.8° N, 12.5° E; Italy) ionospheric station. The ground-based GNSS receiver provides vTEC, while the ionosonde provides *Nm*F2, and we use both of them to calculate τ as:

$$\tau[m] = \frac{\text{vTEC } [el/m^2]}{NmF2\ [el/m^3]}. \tag{1}$$

vTEC values at the ionospheric pierce point altitude of 350 km were obtained through the Ciraolo's calibration method [Ciraolo et al., 2007]. Only GNSS satellites above the 20° cutoff elevation angle have been considered. The Rome GNSS receiver (station code INGR) is part of the *Rete Integrata Nazionale GNSS* (RING, http://ring.gm.ingv.it/) network managed by the *Istituto Nazionale di Geofisica e Vulcanologia* (INGV). Daily *Receiver INdependent EXchange* (RINEX) files, with a time sampling of 30 s, were downloaded from the RING FTP repository (ftp://gpsfree.gm.ingv.it/OUTGOING/RINEX30/RING/). *Nm*F2 values were retrieved from ionograms recorded by the DPS Digisonde [Bibl and Reinisch, 1978] operating in Rome (URSI code RO041) [Upper atmosphere and radiopropagation group et al., 2020]. Ionograms recorded every fifteen minutes were automatically scaled by the *Automatic Real-Time Ionogram Scaler with True height analysis* (ARTIST) software [Galkin and Reinisch, 2008] to get *Nm*F2. Only ionograms with a Confidence Score (C-Score, https://www.ursi.org/files/CommissionWebsites/INAG/web-73/confidence_score.pdf) higher or equal to 75 (out of 100) were considered in this study to discard misinterpreted ionograms [Themens et al., 2022]. Rome ionosonde data can be downloaded from the *electronic Space Weather upper atmosphere* (eSWua) database at http://www.eswua.ingv.it/index.php. Since the time sampling between *Nm*F2 (15 minutes) and vTEC (30 seconds) is different, the procedure developed by Pignalberi et al. [2019] was adopted to provide the vTEC values actually used for τ calculation. Specifically, windows centered at minutes 0, 15, 30, and 45 of each hour (i.e., the ionosonde sampling time) were applied to the 30 s vTEC time series, and only vTEC values falling inside the window were used to calculate the weighted average vTEC value for that specific window. The windows are 15-minute wide, so they do not overlap, and the weight applied is Gaussian with a variance of 2.5 minutes [Pignalberi et al., 2019, 2021]. Therefore, vTEC and *Nm*F2 used for τ calculation have both fifteen-minute time resolution, as the ionosonde time sampling. The vTEC and *Nm*F2 datasets encompass the time range from the beginning of 2001 to the end of 2019, thus covering the years from the maximum of the 23rd solar cycle to the minimum of the 24th solar cycle.

To highlight the main diurnal, seasonal, and solar activity variations of vTEC, *Nm*F2, and τ, the statistical procedure described in Pignalberi et al. [2021, 2022a] was applied. Only magnetically quiet periods were considered by selecting observations inside the following ranges of the *Sym-H* and *AE* geomagnetic activity indices: –25 nT ≤ *Sym-H* ≤ 5 nT and *AE* ≤ 300 nT, as described in Pignalberi et al. [2021, 2022a]. The solar activity variation was highlighted by sorting data as a function of the $F10.7_{81}$ solar activity index. $F10.7_{81}$ is the 81-day running mean of the daily solar radio flux at 10.7 cm wavelength [F10.7, Tapping, 2013]. Specifically, three solar activity ranges were selected:

- Low solar activity (LSA): $F10.7_{81} < 80$ s.f.u. (solar flux unit, 1 s.f.u. = 10^{-22} W m^{-2} Hz^{-1});
- Medium solar activity (MSA): 80 s.f.u. ≤ $F10.7_{81} < 120$ s.f.u.;
- High solar activity (HSA): $F10.7_{81} \geq 120$ s.f.u..

For each solar activity range, data were sorted as a function of the month of the year to highlight the seasonal dependence. Thereafter, the diurnal dependence was highlighted by sorting data in fifteen-minute wide bins in local time (LT). In the end, the original vTEC, *Nm*F2, and τ nineteen-year long time series were split in 3 (solar activity) × 12 (months) × 96 (LT) = 3,456 bins. For each bin we calculated the median value (i.e., the 50th percentile), as representative of their climatological statistical behavior. Grids of fifteen-minute binned median values of vTEC, *Nm*F2, and τ are provided in Section 3.1.

2.2 Slab thickness as modelled by NeQuick

NeQuick is a quick-run empirical model of the ionosphere electron density, the current version of which is NeQuick 2 [Nava et al., 2008, https://t-ict4d.ictp.it/nequick2/nequick-2-web-model]. NeQuick was developed at the *Abdus Salam International Centre for Theoretical Physics* (ICTP), Trieste, Italy, in collaboration with the *Institute for Geophysics, Astrophysics and Meteorology* of the University of Graz, Austria. NeQuick is particularly designed for trans-ionospheric propagation applications and conceived to reproduce the median behavior of the ionosphere, and can be used up to GNSS altitude. The *International Telecommunication Union Radiocommunication sector* (ITU-R) recognized NeQuick 2 as the recommended model for TEC estimation [ITU-R Recommendation P.531-12, 2013]. NeQuick takes as inputs the position, time, and F10.7 solar flux, and gives as output the electron density vertical profile at the given location and time. Furthermore, NeQuick can also provide the electron density along any slant ground-to-satellite ray-path and the corresponding slant TEC (sTEC) by numerical integration. NeQuick describes the electron density profile through a linear combination of six semi-Epstein layers with empirical thickness parameters. The semi-Epstein layers are anchored to the three main ionospheric layers (E, F1, and F2), with different thickness parameters for the bottom and top part of each ionospheric layer.

As mentioned before, NeQuick does not provide τ as a direct output. Nevertheless, τ can be computed as a by-product as the ratio between NeQuick-modelled vTEC and *Nm*F2. Indeed, this is the approach adopted in this study to obtain the NeQuick-modelled τ for positions and times where the corresponding experimentally derived values were available (see Section 2.1). It is understood that the daily F10.7 solar index has been used as a solar activity input for NeQuick. After calculating NeQuick-modelled τ values, they were binned to highlight the main diurnal, seasonal, and solar activity variations, as explained in Section 2.1.

Since the F2-layer, along with its plasmaspheric extension in the topside ionosphere, gives the major contribution to τ, the NeQuick modelling of this ionospheric region is briefly described here. NeQuick F2-layer consists of two semi-Epstein layers describing the electron density N_e as a function of the height h, starting from the F2-layer electron density maximum *Nm*F2, at the height *hm*F2:

$$N_e(h) = 4NmF2\frac{\exp\left(\frac{h-hmF2}{H}\right)}{\left[1+\exp\left(\frac{h-hmF2}{H}\right)\right]^2}. \quad (2)$$

NeQuick derives *Nm*F2 from the ordinary critical frequency *fo*F2 of the F2-layer as modelled by the Jones and Gallet [1962, 1965] spherical harmonics global mapping procedure with CCIR (1967) coefficients. This is the procedure ITU-R compliant [ITU-R Recommendation P.531-12, 2013]. The *hm*F2 modelling is instead based on the Dudeney [1983] formulation.

Eq. (2) is applied for both the topside part (above *hm*F2) and bottomside part (below *hm*F2) of the F2-layer, with different thickness parameters (H). H is a fundamental parameter describing the vertical rate of electron density variation, and then the shape of the electron density profile [Pignalberi et al., 2020a], similarly to the plasma vertical scale height in ionospheric theoretical modelling [Pignalberi et al., 2020b].

In the bottomside F2-layer, the H parameter is called B_{2bot} [Leitinger et al., 2005; Radicella et al., 2021] and is analytically parameterized as:

$$B_{2bot} = \frac{0.04774\, foF2^2}{\left(\frac{dN_e}{dh}\right)_{max}}. \quad (3)$$

B_{2bot} is calculated from *fo*F2 and the electron density vertical derivative at the inflection point $(dN_e/dh)_{max}$ of the semi-Epstein layer representing the bottomside F2 layer. $(dN_e/dh)_{max}$ was empirically modelled by Mosert de Gonzales and Radicella [1990] using ionosonde data as:

$$\left(\frac{dN_e}{dh}\right)_{max} = 0.01\exp[-3.467 + 1.714\ln(foF2) + 2.02\ln(M(3000)F2)], \quad (4)$$

where $M(3000)F2$ is the F2-layer propagation factor for a distance of 3,000 km. Since B_{2bot} does not include any dependence on height, the bottomside F2-layer is assumed to be an ideal semi-Epstein layer.

In the topside F2-layer, H includes also the dependence on height through the formalism developed first by Leitinger et al. [2001, 2002] and Radicella and Leitinger [2001], which then evolved to the current formulation [Coïsson et al., 2006; Nava et al., 2008]:

$$H(h) = H_0 \left[1 + \frac{r \cdot g \cdot (h - hm\mathrm{F2})}{r \cdot H_0 + g \cdot (h - hm\mathrm{F2})}\right], \tag{5}$$

which is dependent on three topside parameters: H_0, g, and r. H_0 is the value assumed by H at the F2-layer peak (hmF2); g is the vertical gradient of H above the F2-layer peak; r is the parameter describing the non-linear asymptotic behavior of H very distant from the F2-layer peak. For more details about the meaning of the NeQuick topside parameters please refer to Pignalberi et al. [2020a]. In Eq. (5), r and g are constant factors equal to 100 and 0.125, respectively. Differently, H_0 is modelled through:

$$H_0 = k \cdot B_{2\mathrm{bot}}, \tag{6}$$

with the parameter k defined as:

$$k = 3.22 - 0.0538\, fo\mathrm{F2} - 0.00664\, hm\mathrm{F2} + 0.113 \frac{hm\mathrm{F2}}{B_{2\mathrm{bot}}} + 0.00257\, R_{12}, \tag{7}$$

where R_{12} is the 12-month running-mean of the sunspot number R. This parameter was empirically determined using experimental topside electron density profiles from topside sounders, mainly ISIS-2 satellite, orbiting at an altitude of 1,400 km during a complete solar cycle [Coïsson et al., 2006].

Eq. (6) represents an explicit link between the bottomside and the topside thickness parameters via the empirical parameter k, which is also dependent on the F2-layer characteristics through Eq. (7). As a consequence, a change of the $B_{2\mathrm{bot}}$ value will affect not only the F2-layer bottomside shape, but also the topside profile shape controlled by the value of H_0, and consequently the vTEC will be very sensitive to its variations.

2.3 Ingestion of observed slab thickness values into the NeQuick model

In order to ingest experimental values of τ into the NeQuick model, a methodology relying on the use of effective parameters and based on simultaneous ingestion of vTEC and F2-layer peak characteristics (NmF2 and hmF2) experimental values has been used [Buresova et al., 2009; Nava et al., 2011].

To briefly describe the ingestion procedure, at a given epoch a GNSS receiver providing vTEC values and a co-located ionosonde providing the relevant NmF2 and hmF2 values are considered. Taking advantage of the ITU-R coefficients and gamma functions implemented into the NeQuick model it is possible to define as *Az_NmF2* the effective solar flux that allows NeQuick to match the experimental NmF2 value. In a similar way, by means of the Dudeney formula [Dudeney, 1983] for hmF2 it is possible to define as *Az_hmF2* the effective solar flux that allows NeQuick to match the experimental hmF2 value. *Az_NmF2* and *Az_hmF2* can therefore be used to constrain the model F2-layer peak as indicated in Fig. 1, where the black curve represents the ionosonde-derived electron density profile at Rome on 5 March 2006 at 13:00 UT (Universal Time), and the green line corresponds to the NeQuick electron density profile after the ingestion of NmF2 and hmF2. Finally, the parameter *B2mod* can be defined as the modulating factor for the $B_{2\mathrm{bot}}$ model parameter that allows NeQuick, driven by *Az_NmF2* and *Az_hmF2*, to match the experimental vTEC and therefore the experimental slab thickness (blue profile in Fig. 1).

For comparison purposes, in the same figure the electron density profile obtained with NeQuick driven by the F10.7 flux of the day (90.7 s.f.u.) and with a vTEC of 13.752 TECU is indicated in red. Considering that the experimental vTEC over the ionosonde is 12.629 TECU and the vTEC related to the model driven by *Az_NmF2* and *Az_hmF2* is 10.632 TECU, it is possible to infer that the NeQuick capability to locally describe the ionospheric peak improves remarkably; nevertheless, as far as the improved description of vTEC and τ are concerned, the introduction of a third effective parameter becomes essential.

Yet, the above definition of the *B2mod* parameter, which can be summarized as in Eq. (8):

$$B2mod = \frac{B_{2\mathrm{bot}}\ (\text{after vTEC assimilation})}{B_{2\mathrm{bot}}\ (\text{before vTEC assimilation})}, \tag{8}$$

allows establishing if NeQuick overestimates or underestimates the ionospheric slab thickness.

In particular, $B2mod > 1$ (< 1) means that the model slab thickness had to be increased (decreased) in order to match the experimental value of τ. A statistical study of the *B2mod* parameter could therefore be used to infer possible improvements in the description of the NeQuick 2 model slab thickness. In Fig.1, after vTEC, *Nm*F2, and *hm*F2 assimilation we obtain the blue profile whose vTEC is 12.558 TECU, which matches the GNSS receiver observed value within 0.1 TECU. $B_{2\mathrm{bot}}$ before vTEC assimilation was 23.4 km and increased to 28.0 km after vTEC assimilation, then $B2mod \sim 1.2$; indeed, the blue profile is thicker than the green one in the F2-layer region and in the overlying topside. It is worth noting that the ionosonde profile (in black) detects the F1-layer presence, which is instead missed by NeQuick (e.g., the blue profile). Anyway, this difference has a negligible impact on the data-assimilation procedure because the difference in vTEC between the black and blue profiles is 0.197 TECU in the range of altitude between 130 and 190 km where the F1-layer occurrence modifies the profile shape.

For completeness, it is mentioned that the *B2mod* parameter in some very specific conditions can reach extreme values (e.g., above 2.5 or below 0.7) which might lead to unrealistic electron density profiles. Nevertheless, the interpretation of the analysis results is not affected by these particular cases. In addition, it has to be noted that *Az_NmF2* and *Az_hmF2* have been used to estimate *fo*F2 and *hm*F2 values with the ITU-R coefficients at a single given location. Nevertheless, this procedure allows estimating the mentioned peak parameters values over a wider region surrounding the ground station, including all the points needed, e.g., to compute a slant TEC. The effective parameters and the modulating factor can therefore be input into NeQuick to (locally) retrieve the ionospheric electron density for the epoch considered. It is understood that in order to accept as inputs two effective parameters related to the solar flux and a coefficient used to modulate the thickness parameter ($B_{2\mathrm{bot}}$) of the NeQuick 2 bottomside profile, the model source code has been heavily modified.

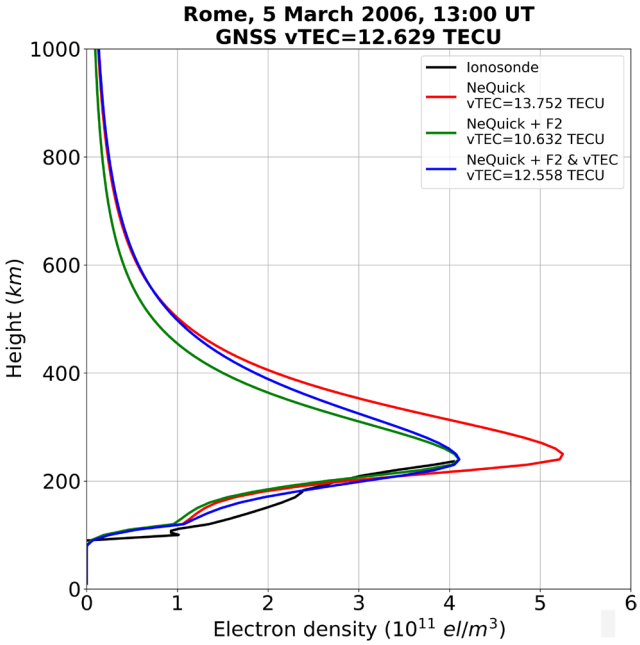

Figure 1. Vertical electron density profiles as measured by the Rome ionosonde for the bottomside region (black curve), and as modelled until an altitude of 1000 km by the original NeQuick (red curve), by NeQuick after assimilation of F2-layer characteristics (green curve), and by NeQuick after assimilating also the vTEC value from co-located ground-based GNSS receiver (blue curve). The example refers to data observed at Rome ionospheric station on 5$^{\mathrm{th}}$ March 2006 at 13:00 UT.

3. Results

3.1 Comparison between measured and NeQuick-modelled slab thickness

In this Section, we compare slab thickness values measured at the Rome mid-latitude ionospheric station with corresponding ones modelled by NeQuick (without any data ingestion), to highlight the main differences for different diurnal, seasonal, and solar activity conditions. Moreover, the same comparison is performed also on vTEC and *Nm*F2 values, which drive the τ variations. The comparison is based on the entire dataset from the beginning of 2001 to the end of 2019, as described in Section 2.1.

Grids of fifteen-minute binned median values of vTEC, *Nm*F2, and τ values measured at the Rome ionospheric station, obtained as described in Section 2.1, are shown in the first column panels of Figs. 2-4, respectively. Corresponding values as modelled by NeQuick, as described in Section 2.2, are shown in the second column panels of Figs. 2-4. Whereas, third column panels show the normalized residuals (in percentage) between modelled and measured values. It is worth noting that τ values represented in Fig. 4 were obtained by applying the statistical procedure described in Section 2.1 to the τ time series obtained through Eq. (1), and not by performing a simple ratio between Fig. 2 and 3 values.

Figure 2 collects the results for vTEC. Measured vTEC shows typical mid-latitude variations concerning the diurnal, seasonal, and solar activity variations [Cesaroni et al., 2021; Tornatore et al., 2021]. vTEC diurnal variation is characterized by highest values during sunlit hours and lowest during night, a pattern that is clearly defined at the

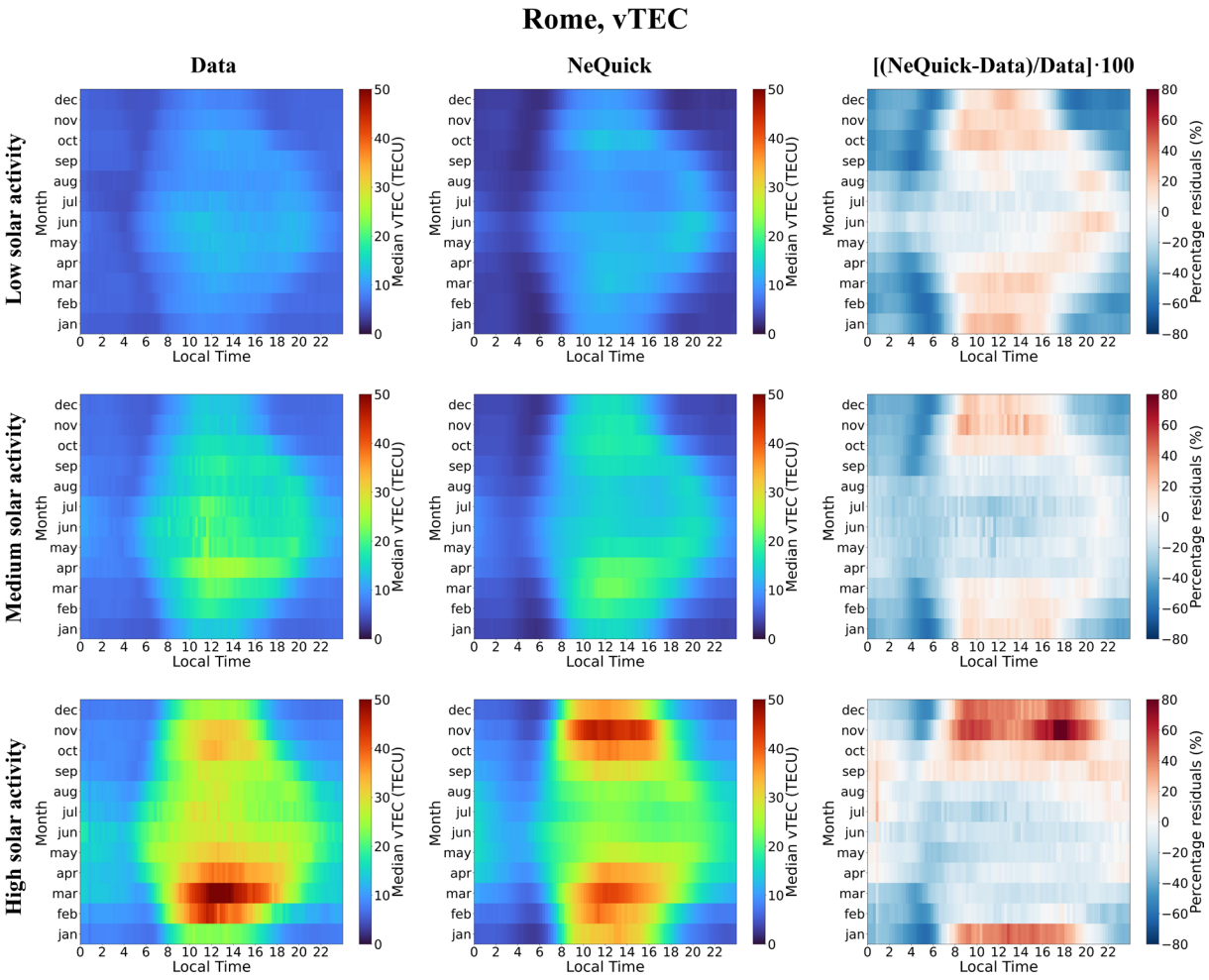

Figure 2. (First column plots) Grids of fifteen-minute binned medians of measured vTEC at Rome for low (top panel), medium (middle panel), and high (bottom panel) solar activity, as a function of LT (*x*-axis) and month of the year (*y*-axis). (Second column plots) Same as the first column but for vTEC values as modelled by NeQuick. (Third column plots) Normalized percentage residuals between modelled and measured vTEC values. The dataset encompasses the years between 2001 and 2019.

LTs of the solar terminator passage at dawn and dusk. vTEC values are positively correlated with the solar activity level, especially during daytime. Measured vTEC at HSA clearly show the semi-annual anomaly with highest values at equinoxes [Zou et al., 2000; Rishbeth et al., 2000], and a clear equinoctial asymmetry with the highest values around the March equinox. The vTEC equinoctial asymmetry for HSA is a feature that NeQuick cannot describe. The comparison between measured and modelled vTEC normalized residuals shows both diurnal, seasonal, and solar activity variations. Given the large vTEC variation in magnitude as a function of solar activity and LT, normalized residuals values provide a more useful and objective statistical metrics than residuals themselves to compare values obtained for very different conditions. Overall, NeQuick underestimates vTEC during nighttime for different seasons. The nighttime underestimation percentually intensifies for LSA. During daytime a seasonal dependence arises, with a slight underestimation in summer and an overestimation in winter, which intensifies for HSA.

Figure 3 collects the results for *Nm*F2, which are typical for mid latitudes [Pietrella et al., 2012]. Since the F2-layer provides a large contribution to vTEC, *Nm*F2 and vTEC share similar features concerning diurnal, seasonal, and solar activity variations. Compared to vTEC, *Nm*F2 shows a clear semi-annual anomaly, which produces larger *Nm*F2 values for equinoxes than for solstices [Fuller-Rowell, 1998; Li and Yu, 2003], also at MSA and LSA, which was clearly visible in vTEC only for HSA. Another remarkable difference between vTEC and *Nm*F2 is that *Nm*F2 does not show the equinoctial asymmetry for HSA during daytime. The semi-annual anomaly in *Nm*F2 is a feature that NeQuick succeeds in describing through the CCIR coefficients. The same for the winter (or seasonal) anomaly which produces highest daytime *Nm*F2 in winter than summer [Zou et al., 2000; Rishbeth et al., 2000]. Normalized residuals do not

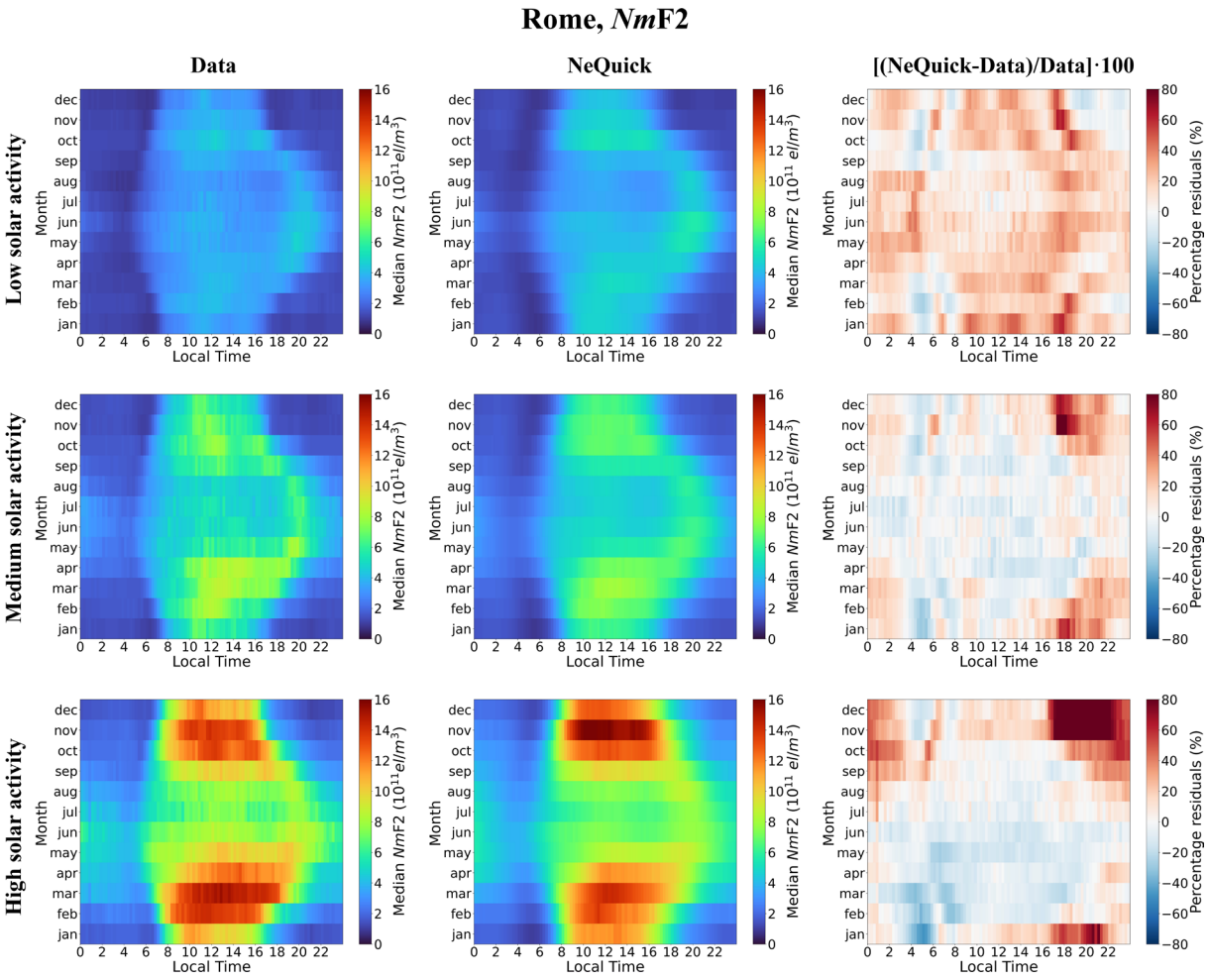

Figure 3. (First column plots) Grids of fifteen-minute binned medians of measured *Nm*F2 at Rome for low (top panel), medium (middle panel), and high (bottom panel) solar activity, as a function of LT (*x*-axis) and month of the year (*y*-axis). (Second column plots) Same as the first column but for *Nm*F2 values as modelled by NeQuick. (Third column plots) Normalized percentage residuals between modelled and measured *Nm*F2 values. The dataset encompasses the years between 2001 and 2019.

show clear diurnal, seasonal, or solar activity trends. For LSA, NeQuick generally overestimates *Nm*F2, while for MSA and HSA a daytime slight underestimation is accompanied by a patchy nighttime overestimation. Remarkable is the large overestimation made by NeQuick for HSA, in winter, for LTs after sunset, where the overestimation exceeds 80%.

Figure 4 collects the results for τ. Measured τ values (first column panels in Fig. 4) show consistent diurnal and seasonal patterns across different solar activity conditions. Daytime hours show the smallest τ (200-300 km) in winter and equinoctial months; instead, τ increases (300-450 km) in summer. Except for the summer season, daytime τ values are smaller than nighttime ones, with the highest τ (450-600 km) observed during nighttime hours in winter. The hours around the solar terminator are characterized by large τ variations, both at dawn and dusk. Features shown by Fig. 4 are representative of the mid-latitudes as described in Pignalberi et al. [2021, 2022a], to which we refer the reader for further information. Differently, NeQuick shows much smaller variations in magnitude with modelled τ values lying in a narrower range between about 220 and 330 km. NeQuick correctly describes the daytime τ seasonal variations with highest values in summer and lowest in winter. Differently, NeQuick underestimates τ during nighttime, except in summer, and the amount of the nighttime underestimation intensifies for LSA. The comparison between vTEC (Figure 2) and τ (Figure 4) normalized residuals clearly demonstrates how vTEC plays a significant role in driving the differences between measured and modelled τ. In fact, vTEC and τ normalized residuals show very similar diurnal, seasonal, and solar activity patterns. This testifies as an accurate modelling of the F2-layer and topside shape, which contributes the most to vTEC, in addition to the F2-layer peak point, is critical for a correct description of τ by empirical models.

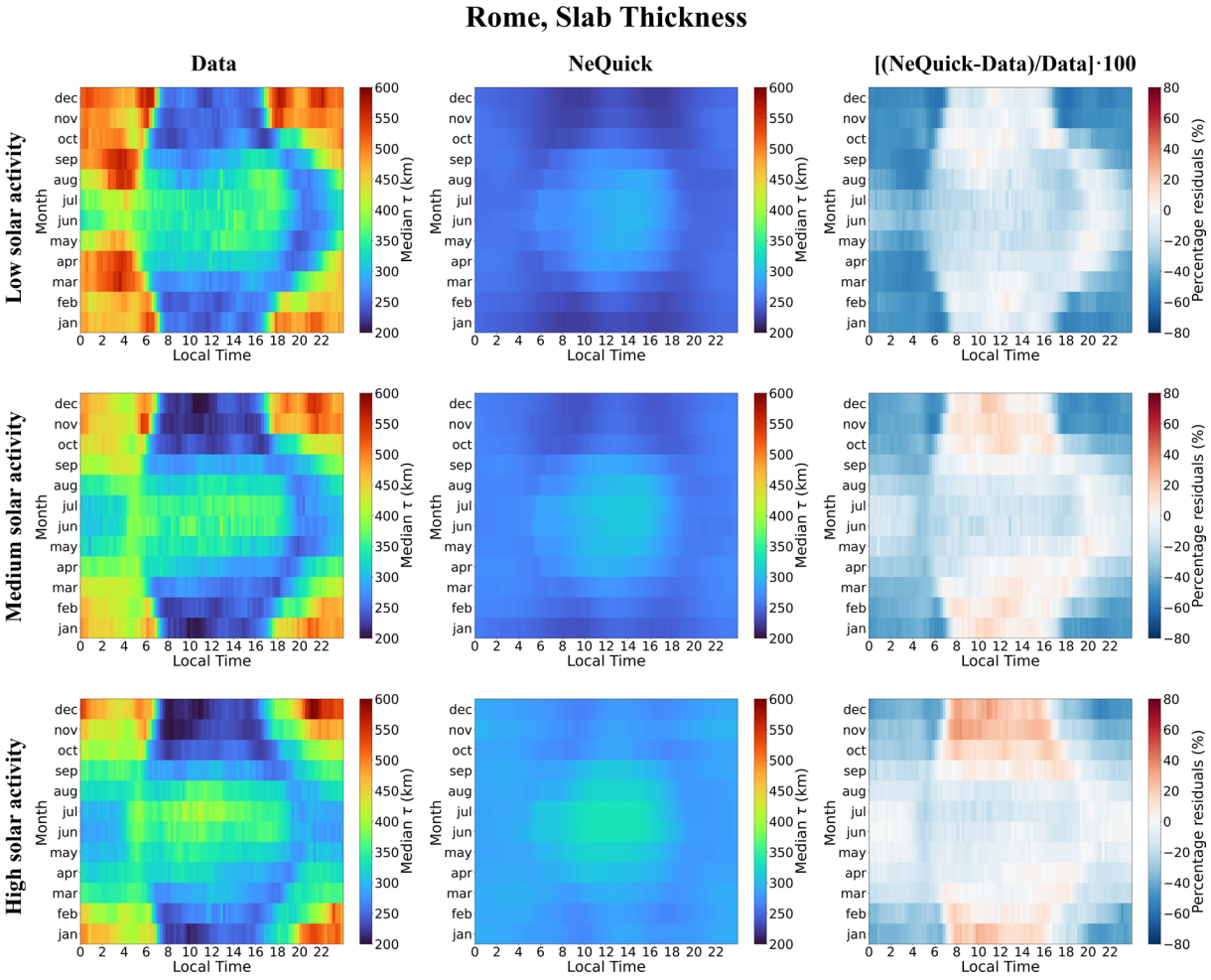

Figure 4 . (First column plots) Grids of fifteen-minute binned medians of measured τ at Rome for low (top panel), medium (middle panel), and high (bottom panel) solar activity, as a function of LT (x-axis) and month of the year (y-axis). (Second column plots) Same as the first column but for τ values as modelled by NeQuick. (Third column plots) Normalized percentage residuals between modelled and measured τ values. The dataset encompasses the years between 2001 and 2019.

3.2 How the ingestion of measured slab thickness modifies the NeQuick profile representation

This Section reports the results on how the NeQuick B_{2bot} parameter has to be modulated through *B2mod*, as described in Section 2.3, to match the ingested vTEC values, and thus the measured τ values after F2-layer characteristics ingestion. For this analysis, we selected three years representative of high (2001), mid (2004), and low (2008) solar activity conditions. For each year, we selected four months representative of the solstices (June and December) and equinoxes (March and September). Values at all LTs were considered. Results for HSA conditions are shown in Fig. 5, while Figs. 6 and 7 show the corresponding results for MSA and LSA, respectively. These are presented as boxplots of thirty-minute binned *B2mod* values as a function of the LT, and as joint probability distributions (JPD) between *B2mod* and corresponding measured τ values for daytime and nighttime conditions. Daytime conditions range between 08:00-16:00 LT, while nighttime conditions range between 22:00-04:00 LT. Table 1 collects the *B2mod* and τ mean and standard deviation values for different solar activity levels and LT sectors as derived from *B2mod* and τ statistical distributions reported in the JPDs of Figs. 5-7.

Figures 5-7 highlight *B2mod* variations with local time, season, and solar activity level. Boxplots show as *B2mod* diurnal variations are remarkable for LSA and decrease as the solar activity increases. In fact, for LSA (Fig. 7), *B2mod* shows a clear diurnal trend characterized by highest values during nighttime and lowest during daytime. During nighttime, *B2mod* mostly ranges between 1.5 and 2.5, while during daytime it ranges between 1.0 and 1.5. The exception to this picture is June (summer season) where the lack of data in the central hours of the day makes it difficult identifying a clear trend. This is due to the extremely high occurrence of Sporadic E layers with blanketing frequency higher than *fo*F2 for the year 2008, which is common at Rome latitude during daytime in summer [Pignalberi et al., 2014, 2015]. Similar diurnal trends characterize the MSA (Figure 6) albeit with a smaller difference between nighttime and daytime values. For these conditions, daytime values are around 1.0 while nighttime values range between 1.5 and 2.0. June month shows a different diurnal trend characterized by *B2mod* values varying between 1.0 and 1.5, regardless of the local time. For HSA (Figure 5), the differences between nighttime and daytime *B2mod* values are even smaller except for December (winter season). *B2mod* diurnal variations represented in the boxplots highlight how, for most of the cases, *B2mod* is higher than 1. As a consequence, NeQuick B_{2bot} needs to be increased to match measured vTEC values, and then τ values. This implies that NeQuick F2-layer thickness parameters are actually underestimated in most of the conditions studied here. The underestimation is particularly evident during nighttime, specifically for LSA conditions, which are the conditions where Fig. 4 shows the most relevant τ underestimation made by NeQuick. This agrees with the comparison shown in Fig. 2 that highlights a nighttime underestimation made by vTEC values modelled by NeQuick. Since *B2mod* values are calculated after matching the F2-layer peak characteristics through ionosonde's measurements ingestion (see Section 2.3), most of the difference between measured and modelled vTEC values has to be attributed to a mismodelling of the F2-layer profile shape and its topside extension through B_{2bot}.

Despite showing large variations with local time, season, and solar activity level, *B2mod* variations are linearly related to the τ magnitude as clearly demonstrated by JPDs in Figures 5-7. Specifically, when measured τ values increase above about 300 km, *B2mod* needs to be largely increased to match the measured vTEC. This is particularly evident during nighttime hours as testified also by *B2mod* and τ mean values reported in Table 1. As shown by Fig. 4, NeQuick modelled τ values never exceed 330 km; as a consequence, the match with measured τ values (often higher than 330 km) requires the modification of the F2-layer profile shape by increasing the layer thickness parameter and then B_{2bot}. For instance, for LSA, equinoctial and winter months, during nighttime, where NeQuick underestimates τ (Figure 4), *B2mod* assumes the highest values between 2.0 and 2.5 (Fig. 7). Differently, where the agreement between measurements and NeQuick is within $\pm$ 10%, as in summer for HSA (Fig. 4), *B2mod* is close to 1, as in the June month panel in Figure 5. In such conditions, NeQuick properly models the ionospheric vertical electron density profile and only slight adjustments in the thickness parameters are necessary to match the observed values.

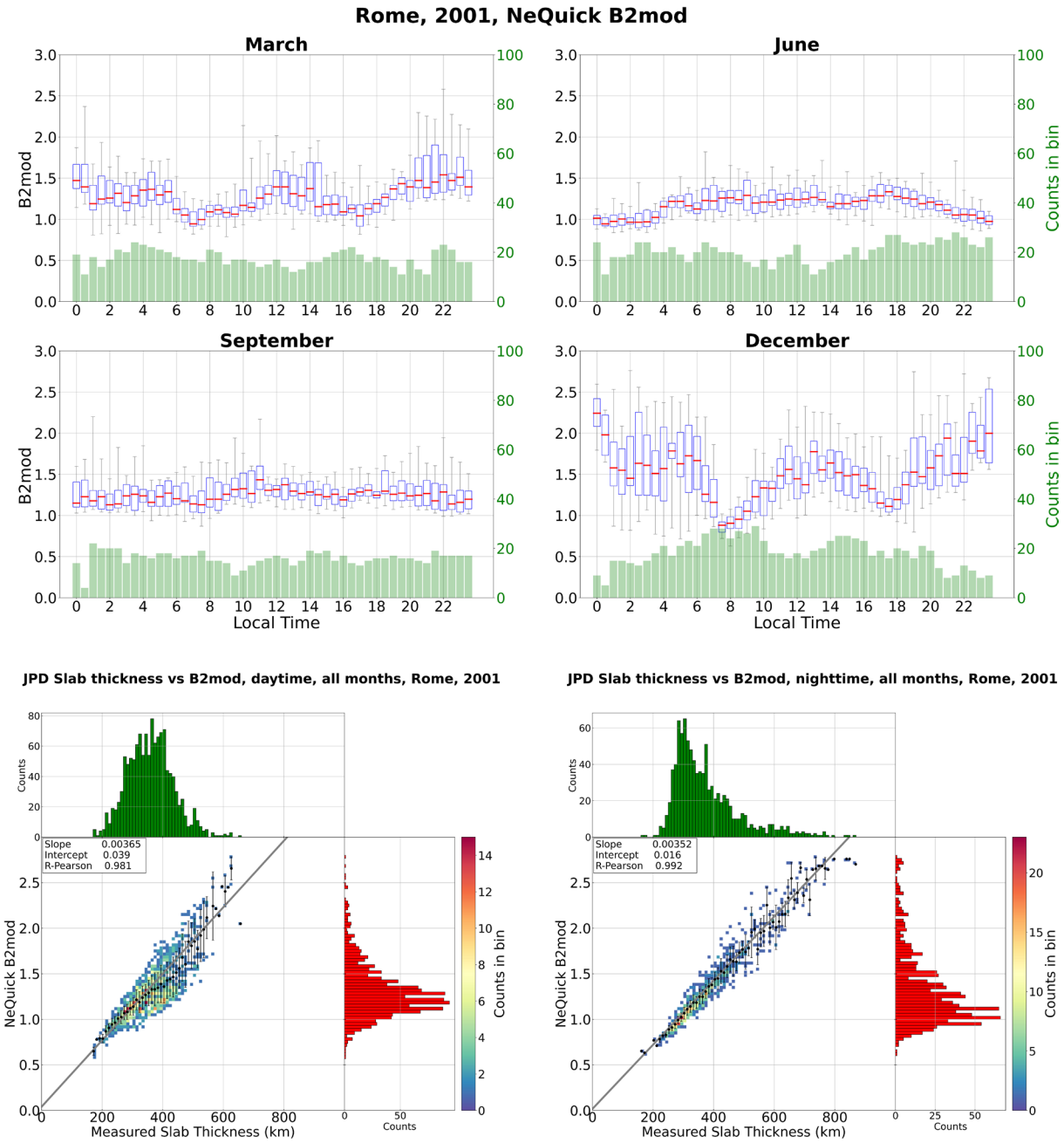

Figure 5. (Top four panels) Boxplots of thirty-minute binned *B2mod* values obtained at Rome, for March, June, September, and December of the year 2001 (HSA), as a function of the LT (*x*-axis). In each boxplot, the red horizontal line is the median value for that bin; the 25th and 75th percentiles are represented in blue as the lower and upper limits of each box, respectively; the 5th and 95th percentiles are shown in grey as lines extending below and above each box (whiskers), respectively. Green shaded bars at the bottom of each panel represent the number of values falling in that bin. (Bottom two panels) Joint probability distributions between measured slab thickness (*x*-axis, green histogram) and NeQuick modelled *B2mod* (*y*-axis, red histogram) values. The black dots refer to the mean values of modelled *B2mod* conditioned by measured slab thickness, with the corresponding standard deviation as error bar. The grey line is the linear fit on black dots, with corresponding coefficients given in the legend. Left plot is for daytime conditions (08:00-16:00 LT), while the right plot is for nighttime conditions (22:00-04:00 LT).

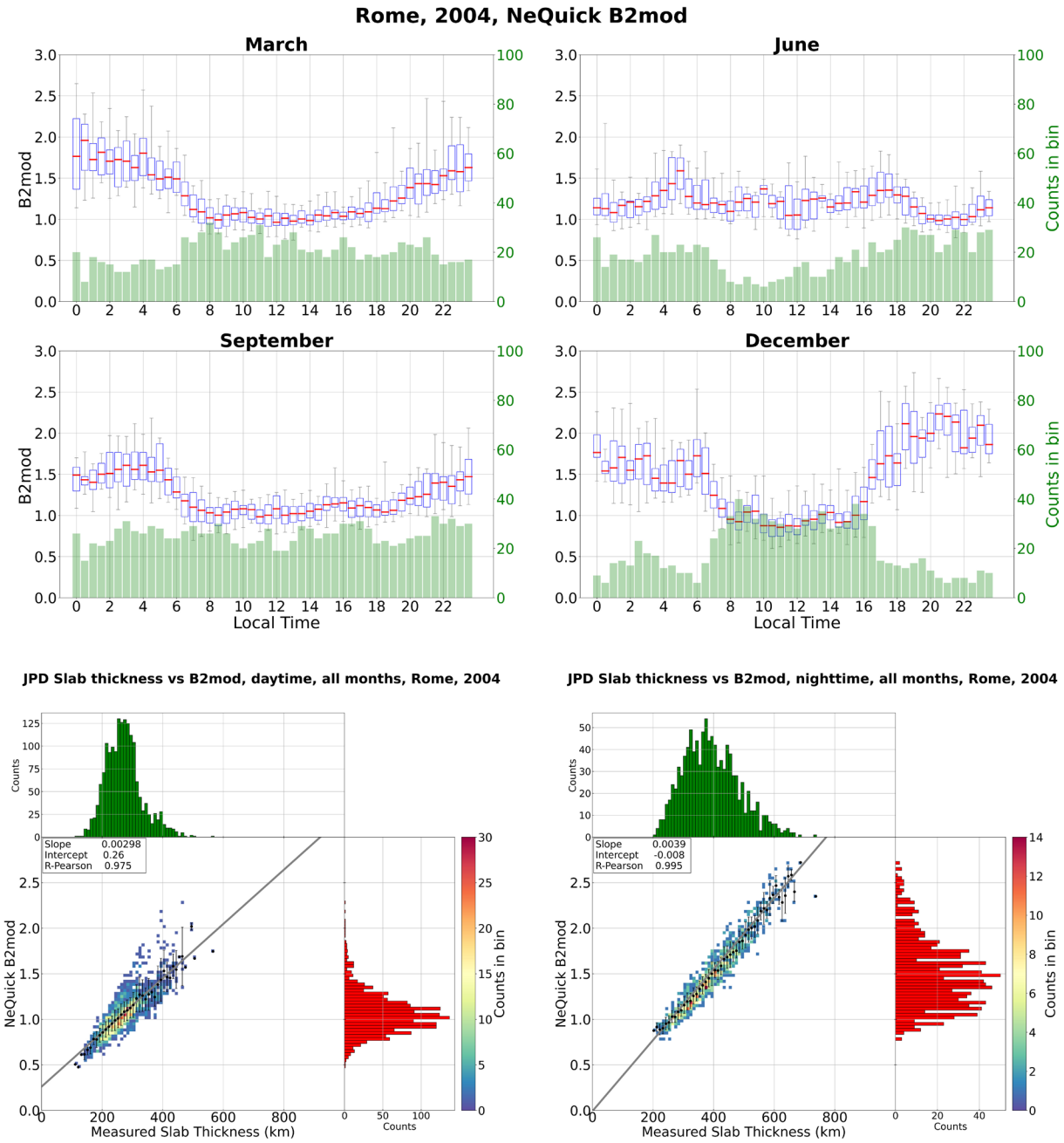

Figure 6. Same as Fig. 5 but for the year 2004 (MSA).

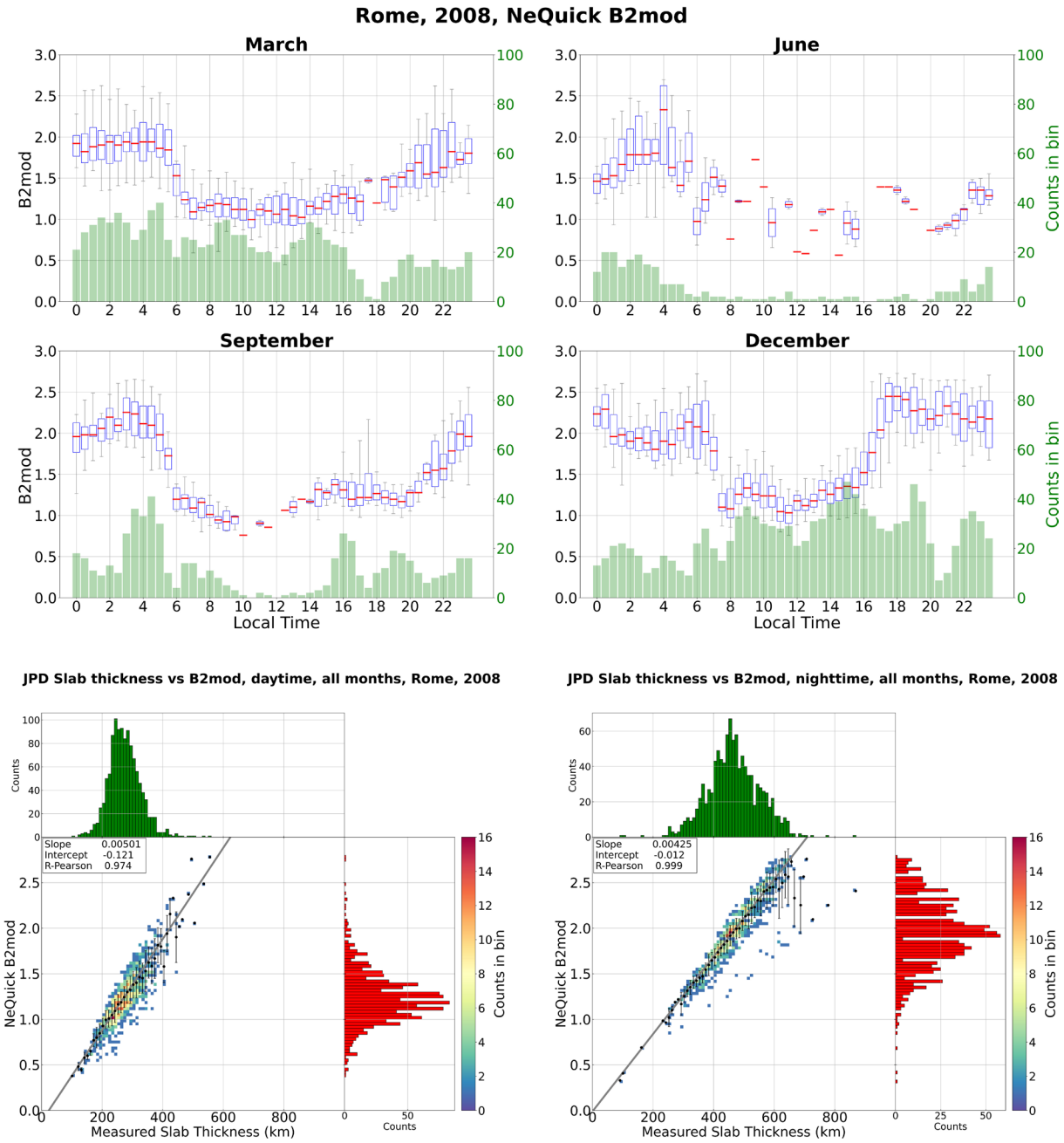

Figure 7. Same as Fig. 5 but for the year 2008 (LSA).

	Daytime (08:00-16:00 LT)		Nighttime (22:00-04:00 LT)	
	B2mod	τ (km)	*B2mod*	τ (km)
HSA (2001)	1.31 ± 0.29	362 ± 77	1.31 ± 0.40	392 ± 148
MSA (2004)	1.04 ± 0.21	269 ± 60	1.48 ± 0.38	396 ± 111
LSA (2008)	1.20 ± 0.25	267 ± 48	1.92 ± 0.38	476 ± 100

Table 1. *B2mod* and τ mean and standard deviation values for different solar activity levels and LT sectors.

4. Discussion

Results of Section 3.1 highlighted how NeQuick modelled values show noticeable differences with both vTEC (Fig. 2) and *Nm*F2 (Fig. 3) observations collected at Rome ionospheric station. As a consequence, these differences characterize the description of τ (Figure 4). Specifically, τ and vTEC normalized residuals between modelled and measured values show very similar diurnal, seasonal, and solar activity variations. This testifies that it is more the description of the vertical electron density profile shape, than that of the F2-layer peak characteristics, that affects the proper modelling of τ by NeQuick. The results of Section 3.2 support this belief and provide concrete indications about possible improvements for the NeQuick τ. In fact, through the three-parameter data assimilation procedure, the F2-layer characteristics (*Nm*F2 and *hm*F2) were constrained with the values measured by ionosonde. As a consequence, after fixing the F2-layer anchor point, most of the differences in both vTEC and τ descriptions have to be attributed to a mismodelling of the bottomside and topside F2-layer profile shape made by NeQuick. This accounts for the *B2mod* variations shown in Fig. 5-7. In particular, to match measured vTEC and τ values, the NeQuick $B_{2\mathrm{bot}}$ parameter needs corrections through *B2mod*, particularly during nighttime at LSA and MSA conditions. Differently, during daytime NeQuick provides a better description of both vTEC and τ, and then $B2mod \sim 1$.

Overall, *B2mod* median values represented in Figs. 5-7 give information about the ability of NeQuick to properly describe the profile shape through the semi-Epstein formulation of Eq. (2) with thickness parameters provided by $B_{2\mathrm{bot}}$ in the bottomside (3), and H in the topside (5). Since $B2mod > 1$ for most of the conditions, NeQuick thickness parameters need to be increased to match observations. Taking into account that in NeQuick the bottomside and topside thickness parameters are bounded by definition through Eq. (6), our analysis cannot discriminate between the bottomside and topside contribution to the *B2mod* correction factor. However, there is experimental and modelling evidence, based on different datasets and methodologies, pointing out that the NeQuick topside representation could be improved by optimizing the description of the topside scale height H. For instance, Kashcheyev and Nava [2019] studied the NeQuick behavior in the topside ionosphere – plasmasphere by comparing vTEC modelled between about 800 km and 20,000 km of altitude with corresponding values provided by COSMIC-1 satellites through precise orbit determination antennas. They found that NeQuick underestimates the vTEC in the topside ionosphere – plasmasphere on average by 3.73 TECU, with variations ranging between 2 and 8 TECU depending on location, local time, season, and solar activity. The overall underestimation found by Kashcheyev and Nava [2019] agrees with *B2mod* median values shown in Figs. 5-7, since the underestimation in vTEC can be solved by increasing the topside scale height H [Pignalberi et al., 2020a], which is possible in NeQuick by increasing H_0 through $B_{2\mathrm{bot}}$, which means to obtain a value of $B2mod > 1$. However, the comparison with only vTEC data does not provide quantitative information on the effect that a mismodelling of the F2-layer peak, which is the anchor point for the topside profile, would produce on the topside profile modelling. More reliable evidence can be obtained by constraining the F2-layer peak through measurements or data-assimilation models, and considering the topside profile shape description. This approach was implemented by Pezzopane and Pignalberi [2019] who inferred a new representation for the NeQuick H_0 parameter by using the IRI UP data-assimilation model for the F2- layer peak anchor point [Pignalberi et al., 2018a] and in-situ N_e values provided by Swarm satellites for the topside anchor point [Pignalberi et al., 2018b]. Making a comparison with vTEC observations from the Swarm B satellite (from about 500 km to the GNSS height), Pezzopane and Pignalberi [2019] evidenced the underestimation by original NeQuick in a range between 3 and 6 TECU depending on solar activity conditions, as found by Kashcheyev and Nava [2019]. With the new representation for the NeQuick H_0 parameter, the underestimation reduces in a range between 2 and 4 TECU. Also in this case, such evidence agrees with our results about *B2mod*. A similar approach has been applied also by Pignalberi et al. [2023] which made use of in-situ N_e values provided by the CSES-01 satellite [Pignalberi et al., 2022c] for the topside anchor point and, in addition, introduced the topside scale height altitudinal variation through COSMIC-1 radio occultation observations. Recently, Pignalberi et al. [2022b] calculated NeQuick topside parameters (H_0, g, and r) through topside profiles obtained from radio occultation by COSMIC-1, with the F2-layer anchor point provided by measurements. These optimized topside parameters were applied to NeQuick by Pezzopane et al. [2023] to study the model behavior at low latitudes in the range of altitudes between *hm*F2 and 850 km. The study highlighted that the original NeQuick underestimates N_e at the DMSP F15 altitude (about 850 km) at low latitudes, but the use of optimized topside parameters, particularly H_0, can face this underestimation. Again, these results point out the importance of improving the NeQuick topside representation, i.e., the topside scale height H, through the optimization of the three NeQuick topside parameters (H_0, g, and r). Hence, even if our analysis

does not allow discriminating the contribution of the bottomside and topside to the *B2mod* variations, the studies above mentioned point out how the topside will probably contribute the most to the *B2mod* variations described in Section 3.2. Moreover, the topside region, including also the plasmasphere contribution up to GNSS satellites altitude (about 20,000 km), gives the largest contribution to vTEC. As a consequence, most of the vTEC and τ variations are due to the topside ionosphere electron content variations. This is particularly evident during nighttime where the contribution from the plasmasphere to vTEC maximizes. In fact, as suggested by Yizengaw et al. [2008] and by Klimenko et al. [2015], the plasmaspheric contribution to vTEC values can reach 10-20% during the day and up to 60% at night, maximizing at low latitudes due to the plasmasphere shape. This accounts for the remarkable difference between measured and modelled τ at night (Fig. 4), and the resultant increase in *B2mod* (Figs. 5-7). This agrees with the studies previously mentioned which evidenced that the topside profile shape changes remarkably from daytime to nighttime conditions; specifically, the topside scale height increases during nighttime, which results in profiles "thicker" around the F2-layer peak and more generally in the topside. We clearly see this effect in the increase of the slab thickness (and, in turn, of *B2mod*) during night-time, especially in the equinoctial and winter seasons.

NeQuick F2-layer bottomside and topside thickness parameters are linked through the k parameter in Eq. (6); as a consequence, the topside and bottomside profiles cannot be modified separately within the current NeQuick formulation. However, several studies highlighted the need of improving the description of the topside profile shape, which is possible through the optimization of the NeQuick topside scale height parameters calculated through in-situ [Pezzopane and Pignalberi, 2019] or radio occultation [Pignalberi et al., 2022b] observations. The proper application of the results described in these studies would require to relax the link between the bottomside and topside thickness parameters in NeQuick, which would be a major change for the model.

5. Conclusions

Nineteen years of ionospheric equivalent slab thickness observations at the mid-latitude ionospheric station of Rome provided us the opportunity to investigate the ability of the NeQuick model to describe this ionospheric parameter, and possibly improve the description of the vertical electron density profile shape made by NeQuick through data assimilation.

The comparison between modelled and measured τ values showed that:

1) NeQuick correctly describes the daytime τ seasonal variations with highest values in summer and lowest in winter; while, during nighttime NeQuick underestimates τ, particularly for LSA, except in summer;
2) NeQuick modelled τ values show much smaller variations in magnitude compared to measurements. They lie in a relatively narrow range between about 220 and 330 km, while measurements reach even 600 km at night;
3) vTEC has the major role in driving the differences between measured and modelled τ values, as testified by vTEC and τ normalized residuals (Figures 2 and 4) showing very similar diurnal, seasonal, and solar activity patterns.

Given the differences between modelled and measured τ values, we tried to assimilate τ values in NeQuick through a three-parameter assimilation procedure based on ionosonde's measured *Nm*F2 and *hm*F2 values, and on vTEC values from a co-located GNSS receiver. After constraining the F2-layer peak anchor point through ionosonde's observations, the assimilation procedure optimizes the NeQuick F2-layer thickness parameter $B_{2\mathrm{bot}}$ through the *B2mod* modulation factor, which derives from the assimilation of measured values of vTEC, and then of τ.

The study of *B2mod* diurnal, seasonal, and solar activity variations showed that:

1) For LSA, *B2mod* presents a clear diurnal trend with highest values (between 1.5 and 2.5) during nighttime and lowest values during daytime (between 1.0 and 1.5). Similar diurnal trends characterize the MSA, except for the summer season, albeit with a smaller difference between nighttime and daytime values. Differently, for HSA this diurnal trend is almost absent, except for the winter season, with values varying between 1.0 and 1.5;
2) In most cases *B2mod* is higher than 1, which implies that the NeQuick $B_{2\mathrm{bot}}$ needs to be increased to match measured values. As a consequence, the NeQuick F2-layer thickness parameters are currently underestimated, particularly during nighttime for LSA;
3) *B2mod* is linearly related to τ. When measured τ values increase above about 300 km, *B2mod* needs to be largely increased to match the measured vTEC values, which means deeply modifying the F2-layer profile shape by increasing $B_{2\mathrm{bot}}$.

Our analysis highlighted what are the ways to be followed to improve the description of the F2-layer profile shape by NeQuick and consequently the matching with the observed values. However, by definition, the NeQuick bottomside and topside thickness parameters are bounded through Eq. (6). This makes it difficult to evaluate what is the contribution from the bottomside and the topside to the *B2mod* correction factor. Based on the evidence from several studies [Kashcheyev and Nava, 2019; Pezzopane and Pignalberi, 2019; Pezzopane et al., 2023], the topside ionosphere, along with its plasmaspheric extension, should give the major contribution to the vTEC mismodelling. The topside description could be improved through the optimization of the NeQuick topside parameters [Pignalberi et al., 2020a; Pignalberi et al., 2022b]; however, the introduction of these changes would require a deep revision of NeQuick, e.g., by relaxing the link between the bottomside and topside thickness parameters.

Acknowledgements. The authors thank the former Telecommunications/ ICT for Development (T/ICT4D) Laboratory Team, The Abdus Salam International Centre for Theoretical Physics, Trieste, Italy, for developing, maintaining, and making available the NeQuick model (https://t-ict4d.ictp.it/nequick2/nequick-2-web-model).

Data availability. Daily RINEX files for the Rome GNSS receiver were downloaded from the RING FTP repository (ftp://gpsfree.gm.ingv.it/OUTGOING/RINEX30/RING/). *Nm*F2 values retrieved from ionograms recorded by the Rome DPS Digisonde were downloaded from the *electronic Space Weather upper atmosphere* (eSWua) database at http://www.eswua.ingv.it/index.php. NeQuick 2 model is available on request on https://t-ict4d.ictp.it/nequick2/nequick-2-web-model. Solar activity indices are available from OMNIWeb Data Explorer website https://omniweb.gsfc.nasa.gov/form/dx1.html. Geomagnetic activity indices are available from NASA's Space Physics Data Facility of the Goddard Space Flight Center (https://spdf.gsfc.nasa.gov/pub/data/omni/high_res_omni/).

References

Amayenc, P., F. Bertin and V. Papet-Lepine (1971). An empirical relationship between ionospheric equivalent slab thickness and mean gradient of the electron temperature in the F-region, Planet. Space Sci., 19, 10, 1313-1317, https://doi.org/10.1016/0032-0633(71)90185-1.

Bauer, J.J. (1960). Inferred temperature variations at the F2 peak, J. Geophys. Res., 65, 1685-1690.

Bibl, K. and B.W. Reinisch (1978). The universal digital ionosonde, Radio Sci., 13, 519-530, https://doi.org/10.1029/RS013i003p00519.

Bilitza, D., M. Pezzopane, V. Truhlik, D. Altadill, B.W. Reinisch and A. Pignalberi (2022). The International Reference Ionosphere model: A review and description of an ionospheric benchmark, Rev. Geophys., 60, e2022RG000792, https://doi.org/10.1029/2022RG000792.

Buresova, D., B. Nava, I. Galkin, M. Angling, S.M. Stankov and P. Coisson (2009). Data ingestion and assimilation in ionospheric models, Ann. Geophys, 52, 3-4, 235-253, https://www.annalsofgeophysics.eu/index.php/annals/article/view/4575.

CCIR (1967). Atlas of ionospheric characteristics, Report 340. Consultative Committee on International Radio, International telecommunication Union.

Cesaroni, C., L. Spogli and G. De Franceschi (2021). IONORING: real-time monitoring of the total electron content over Italy, Remote Sensing, 13, 16, 3290, https://doi.org/10.3390/rs13163290.

Ciraolo, L., F. Azpilicueta, C. Brunini, A. Meza and S.M. Radicella (2007). Calibration errors on experimental slant total 1041 electron content (TEC) determined with GPS, J. Geod., 81, 2, 111-120, 1042, https://doi.org/10.1007/s00190006-0093-1.

Coïsson, P., S.M. Radicella, R. Leitinger and B. Nava (2006). Topside electron density in IRI and NeQuick: features and limitations, Adv. Space Res., 37, 5, 937-942, https://doi.org/10.1016/j.asr.2005.09.015.

Davies, K. and X.M. Liu (1991). Ionospheric slab thickness in middle and low-latitudes, Radio Sci., 26, 4, 997-1005, 1054, https://doi.org/10.1029/91RS00831.

Dudeney, J.R. (1983). The accuracy of simple methods for determining the height of the maximum electron concentration of the F2-layer from scaled ionospheric characteristics, J. Atm. Terr. Phys., 45, 8-9, 629-640, https://doi.org/10.1016/S0021-9169(83)80080-4.

Fox, M.W., M. Mendillo and J.A. Klobuchar (1991). Ionospheric equivalent slab thickness and its modeling applications, Radio Sci., 26, 2, 429-438, https://doi.org/10.1029/90RS02624.

Fron A., I. Galkin, A. Krankowski, D. Bilitza, M. Hernández-Pajares, B.W. Reinisch, Z. Li, K. Kotulak, I. Zakharenkova, I.V. Cherniak, D.R. Dollase, N. Wang, P. Flisek and A. García-Rigo (2020). Towards cooperative global mapping of the ionosphere: fusion feasibility for IGS and IRI with global climate VTEC maps, Remote Sens., 12, 21, 3531, https://doi.org/10.3390/rs12213531.

Fuller-Rowell, T.J. (1998). The "thermospheric spoon": A mechanism for the semiannual density variation, J. Geophys. Res., 103, A3, 3951-3956, https://doi.org/10.1029/97JA03335.

Furman, D.R. and S.S. Prasad (1973). Ionospheric slab thickness: Its relation to temperature and dynamics, J. Geophys. Res., 78, 25, 5837-5843, doi:10.1029/JA078i025p05837.

Galkin, I.A. and B.W. Reinisch (2008). The new ARTIST 5 for all digisondes. Ionosonde Network Advisory Group Bulletin 69, https://www.ursi.org/files/CommissionWebsites/INAG/web-69/2008/artist5-inag.pdf.

Galkin, I., A. Fron, B.W. Reinisch, M. Hernández-Pajares, A. Krankowski, B. Nava, D. Bilitza, K. Kotulak, P. Flisek, Z. Li, N. Wang, D.R. Dollase, A. García-Rigo and I. Batista (2022). Global monitoring of ionospheric weather by GIRO and GNSS data fusion, Atmosphere 13, 371, https://doi.org/10.3390/atmos13030371.

Garriott, O.K. (1960). The determination of ionospheric electron content and distribution from satellite observations: 2. Results of the analysis, J. Geophys. Res., 65, 4, 1151-1157, https://doi.org/10.1029/JZ065i004p01151.

Garriott, O.K., F.L. Smith and P.C. Yuen (1965). Observations of ionospheric electron content using a geostationary satellite, Planet. Space Sci., 13, 8, 829-838, https://doi.org/10.1016/0032-0633(65)90119-4.

Gerzen, T., N. Jakowski, V. Wilken and M.M. Hoque (2013). Reconstruction of F2 layer peak electron density based on operational vertical total electron content maps, Annales Geophysicae, 31, 1241-1249. https://doi.org/10.5194/angeo-31-1241-2013.

Gulyaeva, T.L. and I. Stanislawska (2005). Night-day imprints of ionospheric slab thickness during geomagnetic storm, J. Atmos. Sol. Terr. Phys., 67, 14, 1307-1314, https://doi.org/10.1016/j.jastp.2005.07.006.

Guo, P., X. Xu and G.X. Zhang (2011). Analysis of the ionospheric equivalent slab thickness based on ground-based GPS/TEC and GPS/COSMIC RO measurements, J. Atmos. Terr. Phys., 73, 7-8, 839-846, https://doi.org/10.1016/j.jastp.2011.02.002.

Hibberd, F.H. and W.J. Ross (1966). Total electron content of the ionosphere in middle latitudes, J. Geophys. Res., 71, 9, 2243-2253, https://doi.org/10.1029/JZ071i009p02243.

Huang, H., L. Liu, Y. Chen, H. Le and W. Wan (2016). A global picture of ionospheric slab thickness derived from GIM TEC and COSMIC radio occultation observations, J. Geophys. Res. Space Phys., 121, 867-880, https://doi.org/10.1002/2015JA021964.

ITU-R Recommendation P.531-12 (2013). Ionospheric propagation data and prediction methods required for the design of satellite services and systems, Geneva, 2013, https://www.itu.int/dms_pubrec/itu-r/rec/p/R-REC-P.531-12-201309-S!!PDF-E.pdf.

Jakowski, N., M.M. Hoque, J. Mielich and C. Hall (2017). Equivalent slab thickness of the ionosphere over Europe as an indicator of long term temperature changes in the thermosphere, J. Atmos. Sol. Terr. Phys., 163, 91-102, https://doi.org/10.1016/j.jastp.2017.04.008.

Jakowski, N. and M.M. Hoque (2021). Global equivalent slab thickness model of the earth's ionosphere. J Space Weather Space Clim., 11, 10, https://doi.org/10.1051/swsc/2020083.

Jayachandran, B., T.N. Krishnankutty and T.L. Gulyaeva (2004). Climatology of ionospheric slab thickness, Ann. Geophys., 22, 25-33, https://doi.org/10.5194/angeo-22-25.

Jin, S., J.H. Cho and J.U. Park (2007). Ionospheric slab thickness and its seasonal variation observed by GPS, J. Atmos. Sol. Terr. Phys., 69,1864-1870, https://doi.org/10.1016/j.jastp.2007.07.008.

Jones, W.B. and R.M. Gallet (1962). Representation of diurnal and geographical variations of ionospheric data by numerical methods. J. Res. Natl. Bur. Stand., 66, 129-147, https://doi.org/10.6028/jres.066D.043.

Jones, W.B. and R.M. Gallet (1965). Representation of diurnal and geographic variations of ionospheric data by numerical methods, II. Control of instability, ITU Telecommun. J., 32, 18-28.

Kashcheyev, A. and B. Nava (2019). Validation of NeQuick 2 model topside ionosphere and plasmasphere electron content using COSMIC POD TEC, J. Geophys. Res. Space Phys., 124, 9525-9536, https://doi.org/10.1029/2019JA026971.

Klimenko, M., V.V. Klimenko, I.E. Zakharenkova and I.V. Cherniak (2015). The global morphology of the plasmaspheric electron content during Northern winter 2009 based on GPS/COSMIC observation and GSM TIP model results, Adv. Space Res., 55(8), 2077-2085, https://doi.org/10.1016/j.asr.2014.06.027.

Krankowski, A., I.I. Shagimuratov and L.W. Baran (2007). Mapping of foF2 over Europe based on GPS-derived TEC data, Adv. Space Res., 39, 5, 651-660, https://doi.org/10.1016/j.asr.2006.09.034.

Leitinger, R., B. Nava, G. Hochegger and S. Radicella (2001). Ionospheric profilers using data grids, Phys. Chem. Earth – Part C: Sol. Terr. Plan. Science, 26, 5, 293-301, https://doi.org/10.1016/S1464-1917(01)00002-2.

Leitinger, R., S. Radicella, G. Hochegger and B. Nava (2002). Diffusive equilibrium models for the height region above the F2 peak, Adv. Space Res., 29, 6, 809-814, https://doi.org/10.1016/S0273-1177(02)00036-4.

Leitinger, R., L. Ciraolo, L. Kersley, S.S. Kouris and P. Spalla (2004). Relations between electron content and peak density-regular and extreme behavior, Ann. Geophys., 47, 2/3,1093-1107, https://doi.org/10.4401/ag-3287.

Leitinger, R., M.L. Zhang and S.M. Radicella (2005). An improved bottomside for the ionospheric electron density model NeQuick, Ann. Geophys., IT 48, 3, https://doi.org/10.4401/ag-3217.

Li, X. and T. Yu (2003). Annual and semi-annual variations of the observed *fo*F2 in a high solar activity year, Terr. Atmos. Oceanic Sci., 14, 1, 41-62, doi: 10.3319/TAO.2003.14.1.41(A).

Mosert de Gonzales, M. and S.M. Radicella (1990). On a characteristic point at the base of F2 layer in the ionosphere, Adv. Space Res., 10, 11, 17-25, https://doi.org/10.1016/0273-1177(90)90300-O.

Nava, B., P. Coïsson and S.M. Radicella (2008). A new version of the NeQuick ionosphere electron density model, J. Atmos. Sol. Terr. Phys., 70:1856-1862, https://doi.org/10.1016/j.jastp.2008.01.015.

Nava, B., S.M. Radicella and F. Azpilicueta (2011). Data ingestion into NeQuick 2, Radio Sci., 46, RS0D17, https://doi.org/10.1029/2010RS004635.

Pezzopane, M. and A. Pignalberi (2019). The ESA Swarm mission to help ionospheric modeling: A new NeQuick topside formulation for midlatitude regions, Sci. Rep., 9, 1, 12253, https://doi.org/10.1038/s41598-019-48440-6.

Pezzopane, M., A. Pignalberi and B. Nava (2023). On the low-latitude NeQuick topside ionosphere mismodelling: The role of parameters H0, g, and r, Adv. Space Res., 72, 4, 1224-1236, https://doi.org/10.1016/j.asr.2023.04.014.

Pietrella, M., M. Pezzopane and C. Scotto (2012). Variability of *fo*F2 over Rome and Gibilmanna during three solar cycles (1976-2000), J. Geophys. Res., 117, A05316, doi:10.1029/2011JA017462.

Pignalberi, A., M. Pezzopane and E. Zuccheretti (2014). Sporadic E layer at mid-latitudes: average properties and influence of atmospheric tides, Annales Geophysicae, 32, 1427-1440, https://doi.org/10.5194/angeo-32-1427-2014.

Pignalberi, A., M. Pezzopane and E. Zuccheretti (2015). A spectral study of the mid-latitude sporadic E layer characteristic oscillations comparable to those of the tidal and the planetary waves, J. Atm. Sol. Terr. Phys., 122, 34-44, https://doi.org/10.1016/j.jastp.2014.10.017.

Pignalberi, A., M. Pezzopane, R. Rizzi and I. Galkin (2018a). Effective solar indices for ionospheric modeling: A review and a proposal for a real-time regional IRI, Surv. Geophys., 39, 1, 125-167, https://doi.org/10.1007/s10712-017-9453-z.

Pignalberi, A., M. Pezzopane and R. Rizzi (2018b). Modeling the lower part of the topside ionospheric vertical electron density profile over the European region by means of Swarm satellites data and IRI UP method, Space Weather, 16, 304-320, https://doi.org/10.1002/2017SW001790.

Pignalberi, A., J.B. Habarulema, M. Pezzopane and R. Rizzi (2019). On the development of a method for updating an empirical climatological ionospheric model by means of assimilated vTEC measurements from a GNSS receiver network, Space Weather, 17, 1131-1164, https://doi.org/10.1029/2019SW002185.

Pignalberi, A., M. Pezzopane, D.R. Themens, H. Haralambous, B. Nava and P. Coïsson (2020a). On the analytical description of the topside ionosphere by NeQuick: Modeling the scale height through COSMIC/FORMOSAT-3 selected data, IEEE J. Sel. Topics Appl. Earth Observ. Remote Sens., 13, 1867-1878, https://doi.org/10.1109/JSTARS.2020.2986683.

Pignalberi, A., M. Pezzopane, B. Nava and P. Coïsson (2020b). On the link between the topside ionospheric effective scale height and the plasma ambipolar diffusion, theory and preliminary results, Sci. Rep., 10, 1, 17541, https://doi.org/10.1038/s41598-020-73886-4.

Pignalberi, A., B. Nava, M. Pietrella, C. Cesaroni and M. Pezzopane (2021). Mid-latitude climatology of the ionospheric equivalent slab thickness over two solar cycles, J. Geod., 95, 124, https://doi.org/10.1007/s00190-021-01577-7.

Pignalberi, A., M. Pietrella, M. Pezzopane, B. Nava and C. Cesaroni (2022a). The Ionospheric Equivalent Slab Thickness: A Review Supported by a Global Climatological Study Over Two Solar Cycles, Space Sci. Rev., 218, 37, https://doi.org/10.1007/s11214-022-00909-z.

Pignalberi, A., M. Pezzopane and B. Nava (2022b). Optimizing the NeQuick Topside Scale Height Parameters Through COSMIC/FORMOSAT-3 Radio Occultation Data, IEEE Geoscience and Remote Sensing Letters, 19, 1-5, 8017005, doi: 10.1109/LGRS.2021.3096657.

Pignalberi, A., M. Pezzopane, I. Coco, M. Piersanti, F. Giannattasio, P. De Michelis, R. Tozzi and G. Consolini (2022c). Inter-Calibration and Statistical Validation of Topside Ionosphere Electron Density Observations Made by CSES-01 Mission. Remote Sensing, 14, 18, 4679, https://doi.org/10.3390/rs14184679.

Pignalberi, A., M. Pezzopane, T. Alberti, I. Coco, G. Consolini, G. D'Angelo, P. De Michelis, F. Giannattasio, B. Nava, M. Piersanti and R. Tozzi (2023) Modeling the Topside Ionosphere Effective Scale Height through In Situ Electron Density Observations by Low-Earth-Orbit Satellites. Universe, 9, 280, https://doi.org/10.3390/universe9060280.

Radicella, S.M. and R. Leitinger (2001). The evolution of the DGR approach to model electron density profiles, Adv. Space Res., 27, 1, 35-40, https://doi.org/10.1016/S0273-1177(00)00138-1.

Radicella, S.M., K. Alazo-Cuartas, Y. Migoya-Orué and A. Kashcheyev (2021). Thickness parameters in the empirical modeling of bottomside electron density profiles, Adv. Space Res., 68, 5, 2069-2075, https://doi.org/10.1016/j.asr.2020.12.037.

Rishbeth, H., I.C.F. Müller-Wodarg, L. Zou, T.J. Fuller-Rowell, G.H. Millward, R.J. Moffett, D.W. Idenden and A.D. Aylward (2000). Annual and semiannual variations in the ionospheric F2-layer: II. Physical discussion, Annales Geophysicae, 18, 945-956, https://doi.org/10.1007/s00585-000-0945-6.

Roger, R.S. (1964). Measurements of the equivalent slab thickness of the daytime ionosphere, J. Atmos. Terr. Phys., 26, 4, 475-497, https://doi.org/10.1016/0021-9169(64)90028-5.

Ross, W.J. (1960). The determination of ionospheric electron content from satellite Doppler measurements: 2. Experimental results, J. Geophys. Res., 65, 2607-2615, https://doi.org/10.1029/JZ065i009p02607.

Stankov, S.M. and N. Jakowski (2006). Topside ionospheric scale height analysis and modelling based on radio occultation measurements, J. Atmos. Sol. Terr. Phys., 68, 2, 134-162, https://doi.org/10.1016/j.jastp.2005.10.003.

Stankov, S.M. and R. Warnant (2009). Ionospheric slab thickness-analysis, modelling and monitoring, Adv. Space Res., 44, 1295-1303, https://doi.org/10.1016/j.asr.2009.07.010.

Tapping, K.F. (2013). The 10.7 cm solar radio flux (*F*10.7). Space Weather, 11, 394-406, https://doi.org/10.1002/swe.20064.

Themens, D.R., B. Reid and S. Elvidge (2022). ARTIST ionogram autoscaling confidence scores: Best practices, Radio Sci. Lett., doi: 10.46620/22-0001.

Titheridge, J.E. (1973). The slab thickness of the mid-latitude ionosphere, Planet. Space Sci., 21, 10, 1775-1793, https://doi.org/10.1016/0032-0633(73)90168-2.

Tornatore, V., C. Cesaroni, M. Pezzopane, M.M. Alizadeh and H. Schuh (2021). Performance evaluation of VTEC GIMs for regional applications during different solar activity periods, using RING TEC values, Remote Sensing, 13, 8, 1470, https://doi.org/10.3390/rs13081470.

Upper atmosphere physics and radiopropagation Working Group; Marcocci, C., M. Pezzopane, E. Pica, V. Romano, D. Sabbagh, C. Scotto and E. Zuccheretti (2020). Electronic Space Weather Upper Atmosphere Database (eSWua) – HF Data, Version 1.0. Istituto Nazionale di Geofisica e Vulcanologia (INGV) August 1, 2020, https://doi.org/10.13127/ESWUA/HF.

Yizengaw, E., M.B. Moldwin, D. Galvan, B.A. Iijima, A. Komjathy and A.J. Mannucci (2008). Global plasmaspheric TEC and its relative contribution to GPS TEC, J. Atmosph. Solar-Terr. Phys., 70, 11-12, 1541-1548, https://doi.org/10.1016/j.jastp.2008.04.022.

Wright, J.W. (1960). A model of the F region above $h_{max}F_2$, J. Geophys. Res., 65, 1, 185-191, https://doi.org/10.1029/JZ065i001p00185.

Zou, L., H. Rishbeth, I.C.F. Müller-Wodarg, A.D. Aylward, G.H. Millward, T.J. Fuller-Rowell, D.W. Idenden and R.J. Moffett (2000). Annual and semiannual variations in the ionospheric F2-layer, I. Modelling, Annales Geophysicae. 18, 927-944, https://doi.org/10.1007/s00585-000-0927-8.

***CORRESPONDING AUTHOR: Alessio PIGNALBERI**,
Istituto Nazionale di Geofisica e Vulcanologia,
Rome, Italy
e-mail: alessio.pignalberi@ingv.it